Astronomical and Astrophysical Transactions (*AApTr*), 2012, Vol. 27, Issue 2, pp. 303–312,
ISSN 1055-6796, Photocopying permitted by license only, ©Cambridge Scientific Publishers

Modeling rings and spirals in barred galaxies using manifolds: morphology and kinematics

M. Romero-Gómez*

Institut d'Estudis Espacials de Catalunya (IEEC), Institut de Ciències del Cosmos (ICC), Dept. Astronomia i Meteorologia, Universitat de Barcelona (UB), Martí i Franquès, 1, E08028 Barcelona, Spain

Received 1 February, 2012

In a series of papers we proposed a theory to explain the formation and properties of rings and spirals in barred galaxies. The building blocks of these structures are orbits trapped by the invariant manifolds of the periodic orbits around the unstable Lagrangian points located near the ends of the bar. Here we give a brief summary of the main results concerning the morphology and the kinematics of observed and theoretical spirals and rings. We compare the ratio of ring diameters in theory and in observations and predict that more elliptical rings will correspond to stronger forcings at and somewhat beyond corotation. We show that the shapes of observed and theoretical spirals agree and predict that stronger non-axisymmetric forcings will drive more open spirals. We compute the line-of-sight velocities along the manifolds and we fit them to a sinusoidal curve, concluding that the sine is not an appropriate curve when computing the position angle of a galaxy. Finally, we consider also gaseous arms and their relations to stellar ones.

Keywords: Barred galaxies; Spiral arms; Rings; Structure; Kinematics

1 Introduction

Spiral arms and rings are spectacular features often seen in barred galaxies. By observing images of barred galaxies, we note that in all cases, both spiral arms and rings seem to be linked to the ends of the bar. Here we present a common framework in which the spiral arms and rings are related to the dynamics of the saddle equilibrium points located at the ends of the bar.

2 The invariant manifolds: brief summary

In order to compute the invariant manifolds, we have to first fix the galactic potential. In the work presented here, the potential is composed of an axisymmetric component

*Email: mromero@am.ub.es

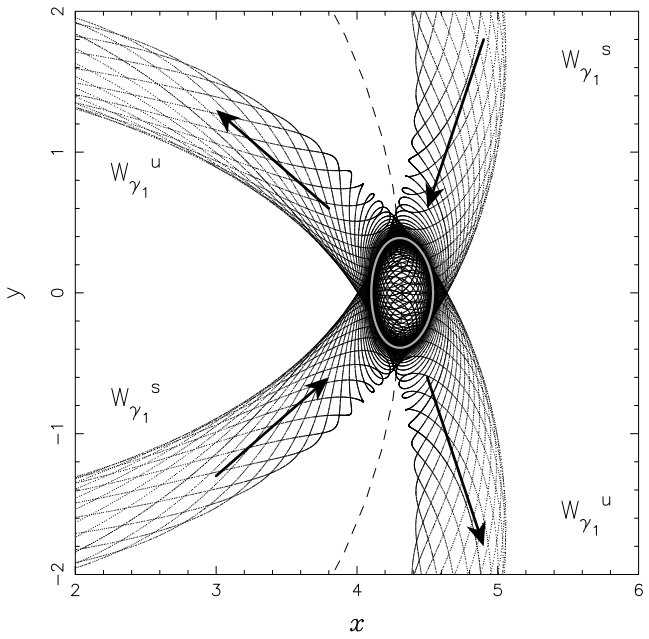


Figure 1 Dynamics around L_1. The four branches of the invariant manifolds (black curves) associated to the Lyapunov orbit (gray curve). The arrows show the sense of circulation, while the black dashed line marks the position of the corotation radius.

and of a bar rotating counter-clockwise with a constant angular velocity, Ω_b[†]. We concentrate on the motion on the $z = 0$ plane (the Galactic plane). The motion in the vertical direction can be essentially described by an uncoupled harmonic oscillator, whose amplitude is relatively small and does not affect the motion in the $z = 0$ plane ([15], hereafter Paper I). We will work in the reference frame where the bar is at rest and we use the convention that in this frame, the bar is along the x-axis.

Our theory is based on the dynamics around the Lagrangian points L_1 and L_2 of a two-dimensional galaxy system. These are located where the first derivatives of the effective potential vanish, on the corotation radius, along the bar semi-major axis and are unstable saddle points [6]. Each of them is surrounded by a family of periodic orbits, called Lyapunov orbits [14]. Since these are unstable they cannot trap around them quasi-periodic orbits of the same energy, so that any orbit in their immediate vicinity (in phase space) will have to escape the neighbourhood of the corresponding Lagrangian point. Not all departure directions are, however, possible. The direction in which the orbit escapes is set by what we call the invariant manifolds. Roughly speaking, these can be thought of as tubes that guide the motion of particles of the same energy as the manifolds [12, 11]. Strictly speaking, they are sets of asymptotic orbits that tend to the Lyapunov orbits as time tends to plus infinity (stable manifold, $W^s_{\gamma_i}$) or as time tends to minus infinity (unstable manifold, $W^u_{\gamma_i}$):

[†]See Appendix for a detailed description of the potentials.

$$\begin{aligned} W^s_{\gamma_i} &= \left\{X \in \mathrm{R}^4 | \lim_{t\to\infty} \parallel \Psi(t,X) - \gamma_i \parallel = 0\right\} \\ W^u_{\gamma_i} &= \left\{X \in \mathrm{R}^4 | \lim_{t\to-\infty} \parallel \Psi(t,X) - \gamma_i \parallel = 0\right\}, \end{aligned}$$

where γ_i is the periodic orbit of a given energy level around the equilibrium point L_i, $i = 1, 2$, and $\Psi(t, X)$ denotes the orbit that has the state $X = (x, y, \dot{x}, \dot{y})$ at $t = 0$. In Fig. 1, we show that from each Lyapunov orbit (light gray thin curve roughly in the middle of the panel), emanate four branches: two of them inside corotation (inner branches) and two of them outside it (outer branches). Along the stable manifolds (one inner and one outer) the mean motion is towards the region of the Lagrangian point, while along the unstable manifolds, it is away from it. In this theory the stars and particles travel along the manifolds.

We need to stress that the terms "stable" and "unstable" do not mean that the orbits that follow them are stable and unstable, respectively. In fact all the orbits that follow the manifold are chaotic, but they are in a loose way "confined" by the manifolds, so that they stay together, at least for a few pattern rotations, in what could be called a bundle. We propose that these manifolds and orbits are the building blocks of the spirals and rings ([16, 2], hereafter Paper II and Paper III, respectively). These manifolds do not exist for all values of the energy, but only for energies for which the corresponding Lyapunov periodic orbit is unstable. This means energies within a range starting from the energy of the L_1 or L_2 (E_{J,L_1}) and extending over a region whose extent depends on the analytic potential [19].

The stable and unstable branches of the invariant manifolds of the same or different periodic orbits can intersect in phase space, thus obtaining a set of orbits called homoclinic, ψ, or heteroclinic, ψ', respectively. They are defined as:

$$\begin{aligned} \psi \quad & s.t. \quad \psi \in W^u_{\gamma_i} \cap W^s_{\gamma_i},\ i = 1, 2, \\ \psi' \quad & s.t. \quad \psi' \in W^u_{\gamma_i} \cap W^s_{\gamma_j},\ i \neq j,\ i, j = 1, 2. \end{aligned}$$

The shape of these orbits in the configuration space remind the shape of the different types of rings. That is, heteroclinic orbits are related to rR_1 rings, where the major axis of the outer ring is perpendicular to the major axis of the bar. Homoclinic orbits are related to R_1R_2 rings, which are galaxies with two outer rings, one with the principal axis perpendicular to the bar major axis, and the other with the axis parallel to the bar. In the cases where no heteroclinic or homoclinic orbits are present, the galaxy presents either two spiral arms emanating from the ends of the bar or, when the outer unstable branches intersect in the (x, y) plane, an outer ring of type R_2. In agreement with [8], the most common structures are the spiral arms and R_1 rings.

3 Main characteristics of the invariant manifolds

The characteristics of the manifolds in external barred galaxies are studied in terms of morphology and kinematics in papers III–V ([3, 4], hereafter Paper IV and Paper V, respectively). The main results can be summarised as follows:

- The strength and the pattern speed of the bar are related to the large-scale structure of the galaxy (Paper III and Fig. 2). We find that weak non-axisymmetric perturbations produce manifolds of rR_1 ring shape, while strong non-axisymmetric perturbations produce spiral arms and other type of rings.

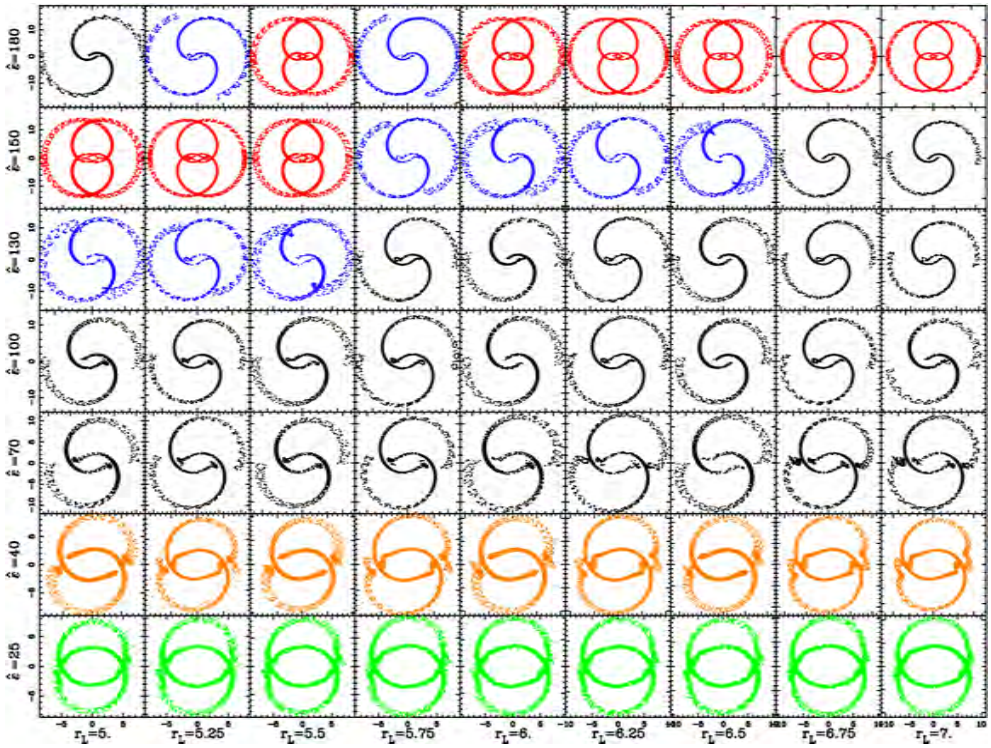


Figure 2 Variation of the bar pattern speed (Ω_b) and the bar amplitude ($\hat{\epsilon}$) in a model with a flat rotation curve and a quadrupole bar. Each panel corresponds to one model. We decrease the pattern speed from left to right and we increase the bar amplitude from bottom to top. The colour code corresponds to rR_1 rings (green), rR_1' pseudo-rings (orange), spirals (black), R_2 rings (blue) and R_1R_2 rings (red).

- The effect of changing the slope of the rotation curve in the outer parts was studied in Paper II. In Fig. 3, we compare the morphologies in two sets of models. In the top panel, all models have a flat rotation curve, while in the bottom panel, the bar parameters are the same but the rotation curve decreases slightly after corotation. Note how the R_1 rings are displaced towards the bottom right corner and more spiral arms are obtained at the top left corner of the figure.
- As for the shape and size of both the inner and outer ring given by the models, we compare the axial ratio of the rings with the values given by the observations (Paper IV). The axial ratio of the inner ring spreads uniformly within the range 0.6–0.95, while the axial ratio of the outer ring falls within the range of 0.7–1 [7]. Besides we find a strong negative correlation between the axial ratio of the rings and the bar strength, given by Q_{t,L_1}, that is, the tangential force of the non-axisymmetric component normalized to the radial force at corotation (left panel of Fig. 5). This correlation is lost if we use, instead, the maximum of the tangential force, $Q_{\rm b}$, as other authors use in the literature to characterise the bar strength.

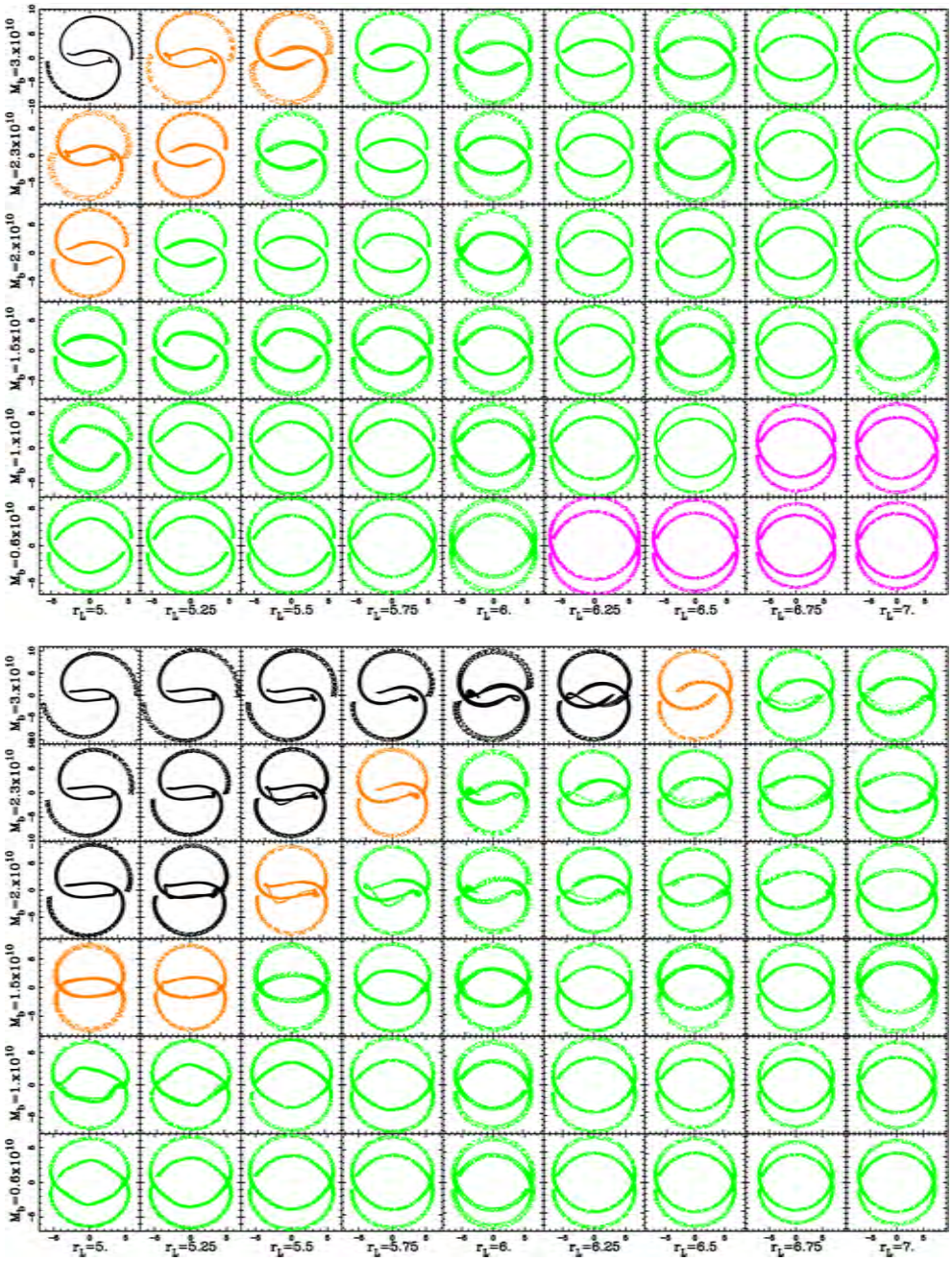


Figure 3 Variation of the bar pattern speed ($\Omega_{\rm b}$) and the bar mass ($M_{\rm b}$) in a model with a Ferrers bar. In the top, the models have a flat rotation curve and in the bottom, the models have a decreasing rotation curve. Each panel corresponds to one model. We decrease the pattern speed from left to right and we increase the bar amplitude from bottom to top. The colour code corresponds to rR_1 rings (green), rR_1' pseudo-rings (orange), spirals (black), circular rings (magenta).

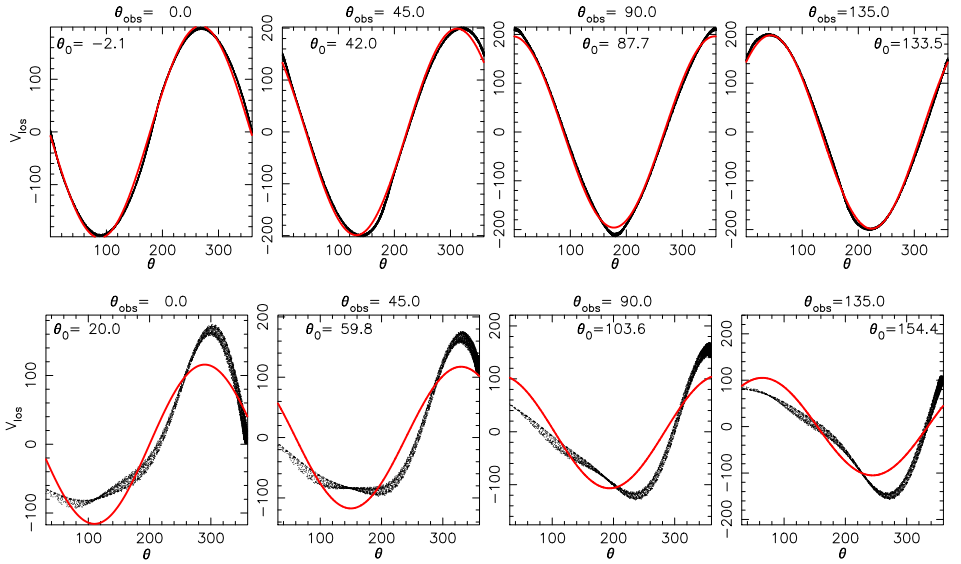


Figure 4 Line-of-sight velocities for four different viewing angles, from left to right: 0°, 45°, 90° and 135°. In each panel we plot in black the velocities given by the orbits trapped by the manifolds as a function of the angle along the manifold, and in red the sinusoidal fit. The value θ_0 indicates the position at which the line-of-sight velocity is zero.

- The default number of spiral arms given by the manifolds is two, since they are associated with the number of saddle points of the model. The typical orientation is trailing, i.e. following the unstable branch of the manifolds, and their shape reproduces the characteristic arm winding often observed in external galaxies (Paper IV).
- The line-of-sight velocities along the R_1 rings fit well a sinusoidal curves of the form $A\sin(\theta-\theta_0)$, no matter the viewing angle, see top panel of Fig. 4, while the line-of-sight velocities along the spirals arms, however, do not fit a sinusoidal curve (bottom panel of Fig. 4). Beware, then, when we use the sin curve to compute the position angle of a galaxy (Paper V).
- We also studied the behaviour of gas with respect to that of the manifolds by simulating collisions of particles trapped by the manifolds by making the particle lose kinetic energy at random positions along the manifold (Paper V). The resulting gaseous arm is somewhat more concentrated than the stellar arm (with any collision), right panel of Fig. 5.
- If the potential is appropriate (i.e., the $m = 4$ component of the Fourier decomposed potential is strong), manifolds can also account for four-armed spirals (Paper III).
- The formation of the manifolds, and therefore of the rings and spirals, depends on the existence of the saddle Lagrangian points. These appear when we perturb the axisymmetric potential with a non-axisymmetric component. We have

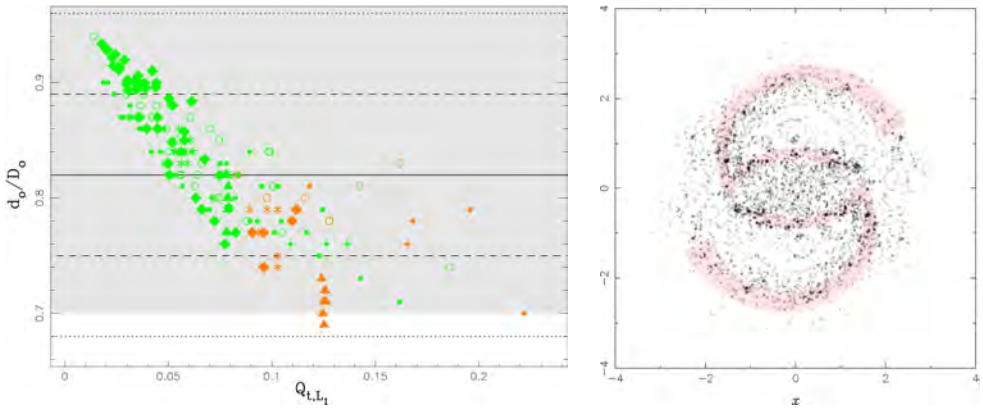


Figure 5 Left panel: axial ratio of the outer ring as a function of the strength parameter, Q_{t,L_1}. The colours are the same as in Figs. 2 and 3. The shaded region is defined by the values obtained from the observation range [7]. The symbols correspond to the different types of bar used. Right panel: the effect of the gas on the manifolds. In black, the results of Schwarz's test particle simulations [17] and in pink, the results of gas-affects manifolds.

applied this theory to barred galaxies, but the saddle Lagrangian points can appear with other non-axisymmetric perturbations, such as spiral perturbations.

4 Conclusions

In a set of papers (Papers I–V) we describe in detail the dynamics given by the invariant manifolds of unstable periodic orbits and how they can be related to the spiral arms and rings in barred galaxies. We perform several tests concerning the shape of the manifolds, that we compare with the available observational data, the kinematics, the effect of the gas, and we give several prediction tools that can be tested in future observational campaigns.

The invariant manifolds described are limited in the sense that they are related to a static system that does not evolve with time, however, they are a good first approximation in order to understand and build the building blocks of the structures. They are different from the density waves, but they are not excluding theories, in the sense that, there may be galaxies better explained with one theory and other that can be explained with the manifolds. One of the main differences is the circulation of the stars in the spiral case. As for the manifolds, they travel along the arms, while in the density waves, they cross the arm in their way towards the outer parts of the disc.

In a word, we present a set of orbits that should be taken into account when modelling a barred galaxy and their spiral arms or rings.

Acknowledgements

This work was supported by the MICINN (Spanish Ministry of Science and Innovation) - FEDER through grant AYA2009-14648-C02-01 and CONSOLIDER CSD2007-00050.

Appendix

In all plots presented here the axisymmetric component consists of the superposition of a Kuz'min/Toomre disc [13, 20] and a spheroid. The surface density of the disc is

$$\sigma(r) = \frac{V_d^2}{2\pi r_d}\left(1+\frac{r^2}{r_d^2}\right)^{-3/2}, \tag{1}$$

where the parameters V_d and r_d set the scales of the velocities and radii, respectively. The spheroid is modelled using a density distribution of the form

$$\rho(r) = \rho_s\left(1+\frac{r^2}{r_s^2}\right)^{-3/2}, \tag{2}$$

where ρ_s and r_s determine its central density and scale length. Although we include two separate axisymmetric components, it is important to note that, in fact, what matters in this study is only the total axisymmetric rotation curve and not its decomposition into components.

Throughout the work we used two types of bar, namely a quadrupole bar [5, 9] and a Ferrers bar [10, 1]. The quadrupole bar is described as the $m = 2$ component of the Fourier decomposition of the potential: $\Phi_b(R,\theta) = A(R)\cos(2\theta)$, where

$$A(R) = A_b\begin{cases}\left(\frac{R}{R_b}\right)^3 - 2, & R \le R_b\\ -\left(\frac{R_b}{R}\right)^3, & R \ge R_b,\end{cases} \tag{3}$$

and R_b and A_b are the size and the amplitude of the bar, in the case of [9] or

$$A(R) = \hat{\epsilon}\sqrt{r}(r_1 - r), \tag{4}$$

in the case of [5], where r_1 is a characteristic scale length of the bar potential and the parameter $\hat{\epsilon}$ is its amplitude.

The Ferrers bar is described by a density distribution with expression:

$$\rho = \begin{cases}\rho_0(1-m^2)^n & m \le 1\\ 0 & m \ge 1,\end{cases} \tag{5}$$

where $m^2 = x^2/a^2 + y^2/b^2$. The values of a and b determine the shape of the bar, a being the length of the semi-major axis, which, in the rotating frame of reference, is placed along the x coordinate axis, and b being the length of the semi-minor axis. The parameter n measures the degree of concentration of the bar. High values of n

correspond to a high concentration, while a value of $n = 0$ is the extreme case of a constant density bar. The parameter ρ_0 represents the central density of the bar. The mass of the bar, $M_{\rm b}$, is equal to

$$M_{\rm b} = 2^{(2n+3)}\pi ab^2\rho_0\Gamma(n+1)\Gamma(n+2)/\Gamma(2n+4)$$

and Γ is the gamma function.

The free parameters that influence most the shape of the manifolds are the mass of the bar, $M_{\rm b}$, in the case of a Ferrers bar, and the bar amplitude, $\hat{\epsilon}$ or $A_{\rm b}$, in the case of a quadrupole bar, which will determine the strength of the bar. The second parameter is the pattern speed, determined by the Lagrangian radius r_L, or distance from the equilibrium point L_1 to the center of the galaxy.

The axisymmetric component describing a flat rotation curve is fixed by setting a maximum disc circular velocity of $164.204\,{\rm km\,s^{-1}}$ at $r = 20$ kpc, and r_s is determined by fixing the total mass of the spheroid and bar components within $r = 10$ kpc to $4.87333 \times 10^{10}\ M_\odot$, while fixing the combined central density of the bar and bulge to $\rho_c = \rho_b + \rho_0 = 2.4 \times 10^{10}\ M_\odot$. More information on these models can be found in [2].

References

[1] Athanassoula, E. 1992, MNRAS, 259, 328
[2] Athanassoula, E., Romero-Gómez, M., Masdemont, J.J. 2009, MNRAS, 394, 67 (Paper III)
[3] Athanassoula, E., Romero-Gómez, M., Bosma, A., Masdemont, J.J. 2009, MNRAS, 400, 1706 (Paper IV)
[4] Athanassoula, E., Romero-Gómez, M., Bosma, A., Masdemont, J.J. 2010, MNRAS, 407, 1433 (Paper V)
[5] Barbanis, B., Woltjer, L. 1967, ApJ, 150, 461
[6] Binney, J., Tremaine, S. 2008, Galactic Dynamics, Second Edition, Princeton Univ. Press, Princeton
[7] Buta, R. 1986, ApJ, 61, 609
[8] Buta, R. 1995, ApJS, 96, 39
[9] Dehnen, W., 2000, AJ, 119, 800
[10] Ferrers N. M. 1877, Q.J. Pure Appl. Math., 14, 1
[11] Gómez, G., Koon, W.S., Lo, M. W., Marsden, J. E., Masdemont, J. J., Ross, S. D. 2004, Nonlinearity, 17, 1571
[12] Koon, W. S. Lo, M. W., Marsden. J. E., Ross, S. D. 2000, Chaos, 10, 2, 427
[13] Kuz'min, G. 1956, Astron. Zh., 33,27
[14] Lyapunov, A. 1949, Ann. Math. Studies, 17
[15] Romero-Gómez, M., Masdemont, J.J., Athanassoula, E., García-Gómez, C. 2006, A& A, 453, 39 (Paper I)
[16] Romero-Gómez, M., Athanassoula, E., Masdemont, J.J., García-Gómez, C. 2007, A& A, 472, 63 (Paper II)
[17] Schwarz, M.P. 1984, MNRAS, 209, 93
[18] Schwarz, M.P. 1985, MNRAS, 212, 677
[19] Skokos, Ch., Patsis, P.A., Athanassoula, E. 2002, MNRAS, 333, 847
[20] Toomre, A. 1963, ApJS, 138, 385
[21] Toomre, A., 1981, in The structure and evolution of normal galaxies, S. M. Fall & D. Lynden-Bell (eds), Proc. of the Advanced Study Institute, Cambridge, England, Cambridge University Press, Cambridge and New York, 111